J Solid State Electrochem (2012) 16:89–92
DOI 10.1007/s10008-010-1282-7

ORIGINAL PAPER

Nitrogen-doped TiO_2 mesosponge layers formed by anodization of nitrogen-containing Ti alloys

Doohun Kim · Hiroaki Tsuchiya · Shinji Fujimoto · Felix Schmidt-Stein · Patrik Schmuki

Received: 4 October 2010 / Revised: 7 December 2010 / Accepted: 8 December 2010 / Published online: 5 January 2011

Abstract An alloy containing 5 at.% of N was produced by arc melting of Ti and TiN powders. By anodization of the alloy in a 10 wt.% K_2HPO_4/glycerol electrolyte at 140 °C, oxide mesosponge layers can be formed with thickness as up to several micrometers. X-ray photoelectron spectroscopy confirms nitrogen uptake in the oxide. Photoelectrochemical measurements show successful N-doping of these mesoporous anodic layers with a significant visible light photoresponse.

Keywords Titanium dioxide · Mesosponges · Photoelectrochemistry · Nitrogen doping · TiN alloy

Introduction

Since Fujishima and Honda demonstrated successful photocatalytic water splitting into H_2 and O_2 using a TiO_2 as a photoanode [1], the field of photocatalysis and photoelectrochemistry using TiO_2 as a semiconductor started flourishing. Although over the years a significant amount of research was dedicated to the subject, a fundamental drawback remained that light-induced redox process on pure TiO_2 could only be activated under UV light irradiation ($\lambda<390$ nm)—this is due to the wide bandgap energy of TiO_2 of ~3.2 eV (for anatase TiO_2 [2]). To extend the spectral photoresponse of TiO_2 to the visible light range, many efforts have been devoted to TiO_2 doping for bandgap engineering [3–9]. TiO_2 can be doped with metal impurities or non-metal atoms. Up to now, non-metal doping has shown the highest improvement in photocatalytic properties compared with other doping approaches, and hence became the most attractive method for TiO_2 modification. Various non-metallic elements (N, C, S, B, P, F, etc.) have been reported to shift the photoresponse threshold of TiO_2 into the visible range. Among all these elements, the most promising approach is N doping. Asahi et al. first demonstrated this N-doping effect by sputtering TiO_2 in an N_2 containing gas [3]. After this discovery, various other approaches have been used, such as direct current magnetron sputtering of TiO_2 electrodes in an $Ar/O_2/N_2$ mixture [10], chemical routes during the precipitation of TiO_2 nanoparticle mixtures [11], ion implantation [12], or annealing in NH_3 gas [13].

In order to reach a high photocatalytic turnover rate, high surface area anodes are desired. Therefore, typically, TiO_2 nanoparticles are sintered to electrodes. However, more recently nanotubular systems showed considerably higher efficiencies (for an overview on TiO_2 nanotubes and their applications, see [9, 14–16]). N-doped TiO_2 nanotubes were successfully formed with ion implantation [12, 17], thermal treatment in an NH_3 gas stream [18, 19], and anodization of TiN alloys [20].

Very recently, we introduced a novel anodization approach which leads to highly defined TiO_2 mesosponge layers [21–24]. In the present work, we explore the feasibility to use a TiN alloy in this anodization process to produce directly N-doped mesoporous titania layer by a single anodization step.

D. Kim · F. Schmidt-Stein · P. Schmuki (✉)
Department of Materials Science, WW4-LKO,
University of Erlangen-Nuremberg,
Martensstr. 7,
91058 Erlangen, Germany
e-mail: schmuki@ww.uni-erlangen.de

H. Tsuchiya · S. Fujimoto
Division of Materials and Manufacturing Science,
Graduate School of Engineering, Osaka University,
2-1 Yamada-oka, Suita,
Osaka 565-0871, Japan

Experimental

The nitrogen-containing titanium alloy (TiN alloy) was prepared from high-purity Ti and TiN powders by using an arc-melting apparatus equipped with a turbo molecular pump (DAIA VAC, Co., Ltd., ACM-01STiN). The TiN alloy contained nominally 5 at.% nitrogen. The alloy ingot was then sawed into slices and, prior to anodization, the surface of the alloy was polished with silicon carbide abrasive paper and 9-μm diamond particle slurries successively to a final finish of colloidal silica suspension. Titanium foils (0.125 mm thickness, 99.6% purity, Advent) were used to produce reference samples (non-doped TiO_2). The polished TiN alloy plates and Ti foils were degreased by sonicating in acetone, isopropanol, and methanol; rinsed with deionized water (DI); and dried in a nitrogen stream.

On the alloy plates and the pure Ti foils, mesosponge layers were produced in an anhydrous electrolyte of 10 wt.% K_2HPO_4/glycerol [21]. Prior to anodization, the electrolyte was heated at 200 °C for 3 h to adjust the water content in the electrolyte. The anodization was carried out using a two electrode system: the degreased Ti foil or TiN alloy plate (working electrode) and a platinum plate (as a counter electrode). The anodization was conducted at a constant voltage of 50 V using a high-voltage potentiostat Jaissle IMP 88 PC. After the anodization, the samples were soaked overnight in DI water, and then dried in a nitrogen stream. To convert the mesosponge layers into anatase, the samples were annealed in air at 450 °C for 1 h with a heating and cooling rate of 30 °C/min using a Rapid Thermal Annealer (Jipelec JetFirst100).

For morphological characterization of the samples, a field-emission scanning electron microscope Hitachi FE-SEM S4800 was used. The cross-section images were taken after scratching the samples.

X-ray diffraction analysis (XRD, X'pert Philips PMD with a Panalytical X'celerator detector) was conducted using graphite monochromized Cu Kα radiation (wavelength 1.54056 Å). Information on the composition and the chemical state were obtained using X-ray photoelectron spectroscopy (XPS, PHI 5600, USA).

Photoelectrochemical characterization was carried out with a set up consisting of a 150 W Xe arc lamp (LOT-Oriel Instruments) as an irradiation source and a cornerstone motorized 1/8 m monochromator. Photocurrent transients were measured directly by opening and closing the monochromator's shutter in the range 600–300 nm with steps of 10 nm wavelength while holding the samples in 0.1 M Na_2SO_4 at a potential of 500 mV (Ag/AgCl).

Results and discussion

Parameter screening experiments showed that for the TiN alloy an anodization for 1 h at a temperature of 140 °C is most successful. This temperature is lower than usually used for pure Ti (180±20 °C) [21–25]. For the alloy, however, severe etching of the formed oxide layer took place at temperatures higher than 140 °C (this leads to the formation of only "thin" and irregular oxide layers). This is in contrast to pure Ti where successful anodization was carried out for 1 h at 200 °C. Figure 1 shows SEM cross-

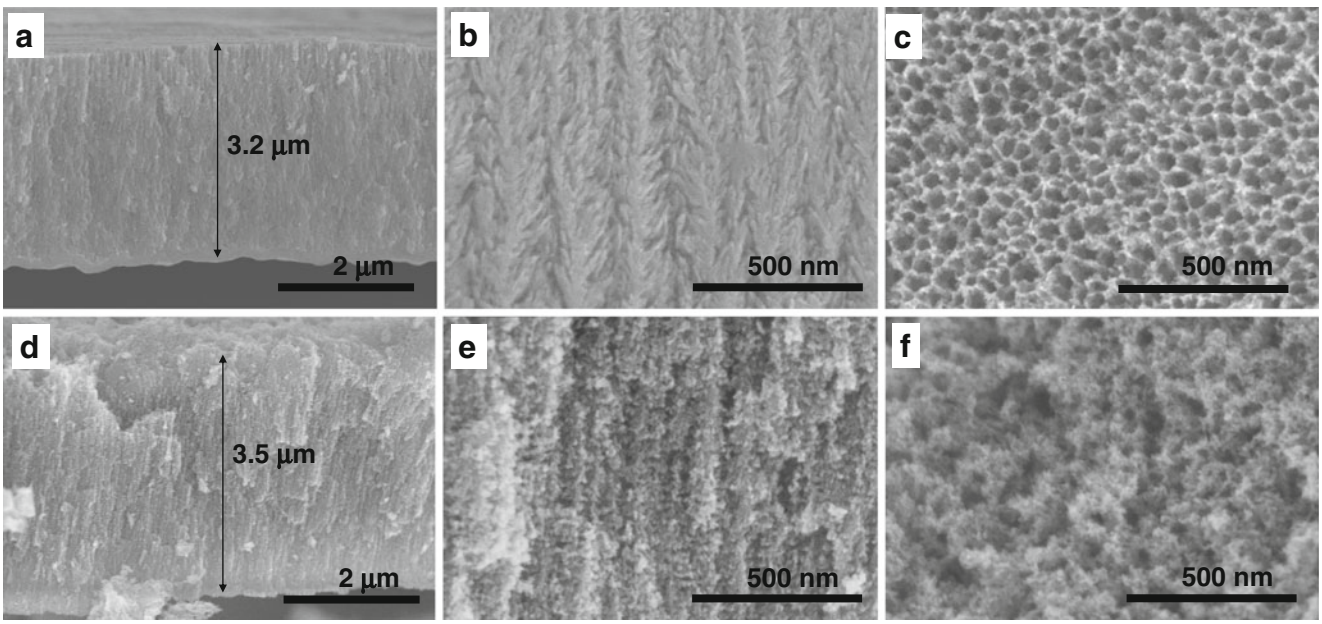

Fig. 1 SEM cross-sectional and top-view images of anodized pure Ti (**a**–**c**) at 200 °C and TiN alloy (**d**–**f**) at 140 °C in 10 wt.% K_2HPO_4/glycerol electrolyte applying constant voltage at 50 V for 1 h. The samples were annealed at 450 °C for 1 h

section and top-view images of the Ti sample (a–c) and the TiN alloy (d–f) after anodization in 10 wt.% K_2HPO_4/glycerol electrolyte at 200 and 140 °C, respectively. In both cases, an approximately 3-μm thick oxide layer was formed that consists of a highly porous structure. The porous channels for the pure TiO_2 are approximately 20 nm, and in the case of the TiN alloy approximately 20–40 nm wide. From the cross-sections, it is apparent that the morphology of the anodized samples shows a "fishbone" structure which is slightly more apparent for the pure TiO_2 mesosponge layer (TMS). For the TiN alloy, the channels form more perpendicular to the alloy substrate over the entire layer thickness, and the top morphology shows a rough surface as shown in Fig. 1d–f. It is remarkable that anodization of the TiN alloy at such comparably low temperature of 140 °C already leads to a formation of thick mesoporous layer on TiN alloy, as for anodization of Ti at this temperature only a compact oxide is obtained. This illustrates how the ability to form mesoporous layers and their morphology strongly depends on the alloying element in Ti.

Figure 2a,b shows the XRD patterns of the samples of the mesosponge layers of Fig. 1 after annealing in air at 450 °C for 1 h. It is evident that anatase/rutile mixed TiO_2 structures (mainly anatase) are observed in both cases. The as-anodized mesosponge samples have typically a mixed amorphous/crystalline structure [21–26]. However, earlier results showed that the amorphous phase is detrimental for photo-induced processes in TiO_2 [27]. Therefore, the sample was annealed at conditions found to be an optimum to transform the layer fully to anatase. Figure 2c shows XPS spectra acquired for the TiN alloy before and after anodization/annealing. Before anodization/annealing (as-polished), the high-resolution peaks for nitrogen 1s were observed at 396 and 400 eV, which represent atomic N as nitride and possibly as oxy-nitride ($TiO_{2-x}N_x$) or absorbed N_2. Asahi et al. reported the N1s XPS peak of O–Ti–N at 396 eV [3], and

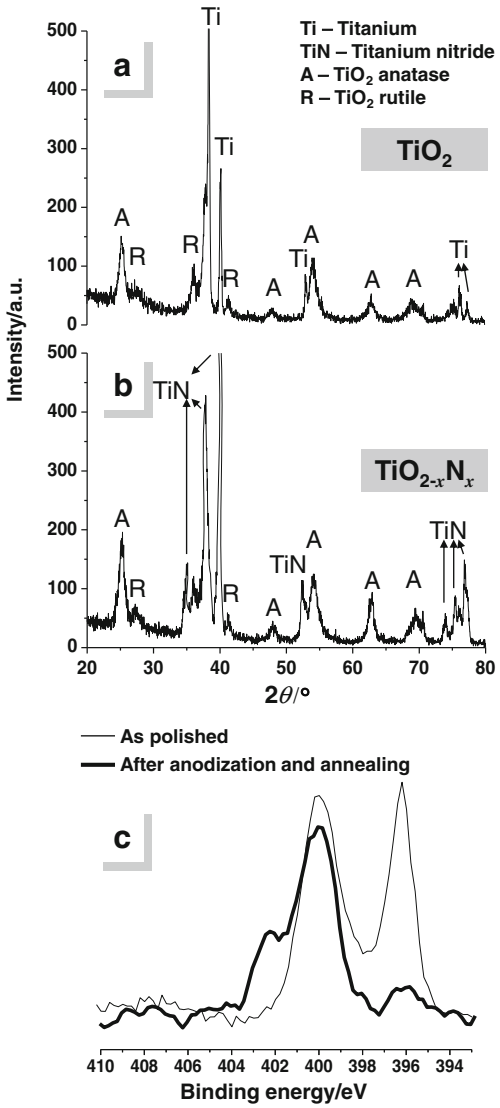

Fig. 2 XRD spectra of the samples anodized with pure Ti (**a**) and TiN alloy (**b**) after annealing in air at 450 °C for 1 h. The peak annotation corresponds to the crystal structure and the original substrates (*A* (anatase), *R* (rutile), *Ti* (titanium), *TiN* (titanium nitride)). **c** XPS spectra (nitrogen 1s) of the TiN alloy before and after anodization/annealing. The spectra are not plotted to the same vertical scale

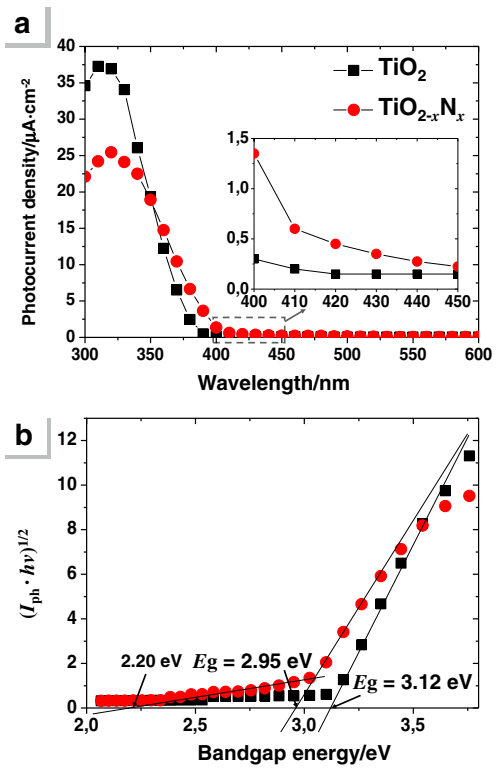

Fig. 3 **a** Photocurrent spectra of the anatase mesosponge TiO_2 and $TiO_{2-x}N_x$ layer anodized with pure Ti and TiN alloy. **b** Evaluation of the bandgap energy (*Eg*) of the anatase TiO_2 and $TiO_{2-x}N_x$ mesosponge layers

literature generally ascribes the peak at 400 eV to N_2 present molecularly chemisorbed on TiO_2 surfaces [28]. After anodization/annealing, except for the peaks at 396 and 400 eV, additionally a shoulder is found at 402 eV. Saha et al. reported that the peak at 402 eV is typical for surface near oxidized states [28]. The peak at 396 eV is assigned to substitutional doping of N for O sites in the TiO_2 lattice, and it is proposed to be most effective for visible light photocatalytic activity. After the anodization/annealing, this peak is still clearly detected with a decreased net intensity.

Figure 3 shows photocurrent spectra that were taken from 600 to 300 nm wavelengths for the annealed anatase TiO_2 and N-doped TiO_2 mesosponge layers of Figs. 1 and 2. It is apparent that the mesosponge layer on pure Ti has a higher response in the UV range. In case of the mesosponge layers on the TiN alloy, the UV response decreases, but at the same time this sample shows a strongly increased photoresponse in the visible range. Figure 3c shows an evaluation of the data according to an indirect bandgap in a $(I_{ph} \cdot h\nu)^{1/2}$ vs. $h\nu$ plot. For the anatase TiO_2, the determined indirect bandgap energy (Eg) results as 3.12 eV as expected. For the $TiO_{2-x}N_x$ mesosponge layers, a primary value for the bandgap of 2.95 eV is obtained; however, a tail down to 2.2 eV is apparent. This bandgap narrowing with a significant visible photoresponse indicates a successful doping of the oxide with nitrogen. In other words, the present results show the feasibility to grow directly anodic N-doped mesoporous oxide structures which may find application in all fields where currently nanoparticulate TiO_2 photoanodes are used. It should be noted that the present approach has the advantage of a strongly interlinked nanoporous network without sintering or compacting particles, and thus yields very stable electrode surfaces.

Conclusions

We used a TiN alloy prepared using arc-melting process to grow, by anodization, a several micrometer thick N-doped TiO_2 mesosponge layer. The results of the photoresponse investigations show that after annealing, nitrogen is successfully incorporated as an active dopant in the crystalline structure of an anatase phase. As a result, these samples show a considerable photoresponse if activated with visible light.

Acknowledgments The authors would like to acknowledge DFG and the Erlangen DFG Cluster of Excellence for financial support, and Helga Hildebrand for valuable technical help.

References

1. Fujishima A, Honda K (1972) Nature 238:37–38
2. Rothenberger G, Moser J, Gratzel M (1985) J Am Chem Soc 107:8054–8059
3. Asahi R, Morkawa T, Ohwaki T, Aoki K, Taga Y (2001) Science 293:269–271
4. Anpo M (1997) Catal Surv Jpn 1:169–179
5. Mills A, LeHunte S (1997) J Photochem Photobiol A 108:1–35
6. Sakthivel S, Kisch H (2003) Angew Chem Int Ed 42:4908–4911
7. Chen X, Mao SS (2007) Chem Rev 107:2891–2959
8. Fujishima A, Zhang X, Tryk DA (2008) Surf Sci Rep 63:515–582
9. Nah YC, Paramasivam I, Schmuki P (2010) Chemphyschem 11:2698–2713
10. Lindgren T, Mwabora JM, Avendano E, Jonsson J, Hoel A, Granvist CG, Lindquist SE (2003) J Phys Chem B107:5709–5716
11. Burda C, Lou Y, Chen X, Samia ACS, Stout J, Gole JL (2003) Nano Lett 3:1049–1051
12. Ghicov A, Macak JM, Tsuchiya H, Kunze J, Haeublein V, Frey L, Schmuki P (2006) Nano Lett 6:1080–1082
13. Kosowska B, Mozia S, Morawski A, Grznil B, Janus M, Kalucki K (2005) Sol Energy Mater Sol Cells 88:269–280
14. Macak JM, Tsuchiya H, Ghicov A, Yasuda K, Hahn R, Bauer S, Schmuki P (2007) Curr Opin Solid State Mater Sci 11:3–18
15. Ghicov A, Schmuki P (2009) Chem Commun 2791–2808
16. Roy P, Berger S, Schmuki P (2010) TiO2 nanotubes—synthesis and applications. Angew Chem Int Ed
17. Ghicov A, Macak JM, Tsuchiya H, Kunze J, Haeublein V, Kleber S, Schmuki P (2006) Chem Phys Lett 419:426–429
18. Vitiello RP, Macak JM, Ghicov A, Tsuchiya H, Dick LFP, Schmuki P (2006) Electrochem Commun 8:544–548
19. Macak JM, Ghicov A, Hahn R, Tsuchiya H, Schmuki P (2006) J Mater Res 21:2824–2828
20. Kim D, Fujimoto S, Schmuki P, Tsuchiya H (2008) Electrochem Commun 10:910–913
21. Kim D, Lee K, Roy P, Birajdar BI, Spiecker E, Schmuki P (2009) Angew Chem Int Ed 48:9326–9329
22. Lee K, Kim D, Roy P, Paramasivam I, Birajdar BI, Spiecker E, Schmuki P (2010) J Am Chem Soc 132:1478–1479
23. Kim D, Roy P, Lee K, Schmuki P (2010) Electrochem Commun 12:574–578
24. Roy P, Dey T, Lee K, Kim D, Fabry B, Schmuki P (2010) J Am Chem Soc 132:7893–7895
25. Habazaki H, Teraoka M, Aoki Y, Skeldon P, Thompson GE (2010) Electrochim Acta 55:3939–3943
26. Lee W, Kim D, Lee K, Roy P, Schmuki P (2010) Electrochim Acta 56:828–833
27. Beranek R, Tsuchiya H, Sugishima T, Macak JM, Taveira L, Fujimoto S, Kisch H, Schmuki P (2005) Appl Phys Lett 87:243114
28. Saha NC, Tompkins HG (1992) J Appl Phys 72:3072–3079